Epilepsy Research 156 (2019) 106110

Contents lists available at ScienceDirect

Epilepsy Research

journal homepage: www.elsevier.com/locate/epilepsyres

Harmonization of pipeline for detection of HFOs in a rat model of post-traumatic epilepsy in preclinical multicenter study on post-traumatic epileptogenesis☆

Cesar Santana-Gomez[a,*,1], Pedro Andrade[b,1], Matthew R. Hudson[c,d,1], Tomi Paananen[b], Robert Ciszek[b], Gregory Smith[e], Idrish Ali[c,d], Brian K. Rundle[a], Xavier Ekolle Ndode-Ekane[b], Pablo M. Casillas-Espinosa[c,d], Riikka Immonen[b], Noora Puhakka[b], Nigel Jones[c,d], Rhys D. Brady[c,d], Piero Perucca[c,d], Sandy R. Shultz[c,d], Asla Pitkänen[b], Terence J. O'Brien[c,d], Richard Staba[a]

[a] Department of Neurology, David Geffen School of Medicine at UCLA, Los Angeles, CA, USA
[b] A.I. Virtanen Institute for Molecular Sciences, University of Eastern Finland, Kuopio, Finland
[c] The Department of Neuroscience, Central Clinical School, Monash University, Melbourne, Australia
[d] Department of Medicine, The Royal Melbourne Hospital, The University of Melbourne, VIC, 3052, Australia
[e] Department of Neurosurgery, David Geffen School of Medicine at UCLA, Los Angeles, CA, USA

ARTICLE INFO

Keywords:
Brain oscillation
Common data element
Electroencephalogram
Traumatic brain injury

ABSTRACT

Studies of chronic epilepsy show pathological high frequency oscillations (HFOs) are associated with brain areas capable of generating epileptic seizures. Only a few of these studies have focused on HFOs during the development of epilepsy, but results suggest pathological HFOs could be a biomarker of epileptogenesis. The Epilepsy Bioinformatics Study for Antiepileptogenic Therapy" (EpiBioS4Rx) is a multi-center project designed to identify biomarkers of epileptogenesis after a traumatic brain injury (TBI) and evaluate treatments that could modify or prevent the development of post-traumatic epilepsy. One goal of the EpiBioS4Rx project is to assess whether HFOs could be a biomarker of post-traumatic epileptogenesis. The current study describes the work towards this goal, including the development of common surgical procedures and EEG protocols, an interim analysis of the EEG for HFOs, and identifying issues that need to be addressed for a robust biomarker analysis. At three participating sites – University of Eastern Finland (UEF), Monash University in Melbourne (Melbourne) and University of California, Los Angeles (UCLA) – TBI was induced in adult male Sprague-Dawley rats by lateral fluid-percussion injury. After injury and in sham-operated controls, rats were implanted with screw and microwire electrodes positioned in neocortex and hippocampus to record EEG. A separate group of rats had serial magnetic resonance imaging after injury and then implanted with electrodes at 6 months. Recordings 28 days post-injury were available from UEF and UCLA, but not Melbourne due to technical issues with their EEG files. Analysis of recordings from 4 rats – UEF and UCLA each had one TBI and one sham-operated control – showed EEG contained evidence of HFOs. Computer-automated algorithms detected a total of 1,819 putative HFOs and of these only 40 events (2%) were detected by all three sites. Manual review of all events verified 130 events as HFO and the remainder as false positives. Review of the 40 events detected by all three sites was associated with 88% agreement. This initial report from the EpiBioS4Rx Consortium demonstrates the standardization of EEG electrode placements, recording protocol and long-term EEG monitoring, and differences in detection algorithm HFO results between sites. Additional work on detection strategy, detection algorithm performance, and training in HFO review will be performed to establish a robust, preclinical evaluation of HFOs as a biomarker of post-traumatic epileptogenesis.

☆ This article is part of a special issue 'Discovery of diagnostic biomarkers for post-traumatic epileptogenesis – an interim analysis of procedures in preclinical multicenter trial EpiBios4Rx'.

* Corresponding author at: David Geffen School of Medicine at UCLA, Department of Neurology, Reed Neurological Research Center, Suite 2155, 710 Westwood Plaza, Los Angeles, CA, 90095, USA.
E-mail address: csantanagomez@mednet.ucla.edu (C. Santana-Gomez).

[1] Contributed equally to this manuscript.

https://doi.org/10.1016/j.eplepsyres.2019.03.008
Received 23 December 2018; Received in revised form 12 March 2019; Accepted 14 March 2019
Available online 15 March 2019

1. Introduction

Studies involving presurgical patients with epilepsy and rodent models of chronic epilepsy induced by status epilepticus show pathological high-frequency oscillations (HFOs; 80–500 Hz) are associated with epileptogenic tissue, and could play a role in generating seizures (for review see Jacobs et al., 2012; Jiruska et al., 2017). Results from studies that recorded EEG immediately after experimental status epilepticus (SE) suggest HFOs could also play a role in the development of epilepsy (Bragin et al., 2004, 2000; Lévesque et al., 2011). The work by Bragin et al. (2004) found little evidence of HFOs after status in rats that did not develop epilepsy, but prominent HFOs were detected in rats that later developed recurrent spontaneous seizures. Moreover, the sooner HFOs were detected, the sooner the first spontaneous seizure occurred (Bragin et al., 2004). These latter data support a hypothesis that pathological HFOs reflect progressive neuronal disturbances after an epileptogenic brain injury and could be a biomarker of epileptgoenesis.

Post-traumatic epilepsy (PTE) is a serious neurological sequela of traumatic brain injury (TBI) and develops in about 16% of cases of severe TBI (Annegers et al., 1998). Currently there are no biomarkers to predict who will develop PTE, which might not manifest until months or years after a TBI. The lack of biomarkers has hindered the development of new treatments that might modify or prevent PTE. However, recent work in a fluid-percussion injury (FPI) rat model of TBI detected pathological HFOs in the perilesional cortex of some, but not all, TBI rats (Bragin et al., 2007). No pathological HFOs were recorded in control rats. In rats that had long-term EEG recordings, rats that had pathological HFOs within two weeks of TBI later developed spontaneous seizures, and none of the rats without these events developed later seizures. Pathological HFOs, similar to those during epileptogenesis in status epilepticus models, might also reflect epileptogenesis in the FPI model.

The Epilepsy Bioinformatics Study for Antiepileptogenic Therapy (EpiBioS4Rx) is a NINDS-funded, international multi-center project designed to identify biomarkers of epileptogenesis and treatments that could modify the development of PTE. One of the goals of this project will be to determine whether HFOs are a biomarker of epileptogenesis in the rat FPI model. A significant aspect of this work involves the standardization of protocols for the FPI model, the electrodes, and the electrode placements; assessing EEG recording capabilities and algorithms for HFO detection and verification; and identifying issues and generating solutions to solve them, which is described in the current report.

2. Materials and methods

Three sites from the international NIH-funded Centre without Walls consortium, the Epilepsy Bioinformatics Study for Antiepileptogenic Therapy (EpiBioS4Rx) (http:// http://epibios.loni.usc.edu/) were involved in the harmonization for EEG recording and HFO analysis in the FPI model. These sites were The University of Eastern Finland (UEF), Monash University in Melbourne (Melbourne) and The University of California, Los Angeles (UCLA).

2.1. Animals

In the three study sites, adult male Sprague-Dawley rats (300–350 g) were used in all experiment. All animal procedures in UEF were approved by the Animal Ethics Committee of the Provincial Government of The Southern Finland and carried out in accordance with the guidelines of the European Community Council Directives 2010/63/EU. Animal procedures in Melbourne were approved by the Florey Animal Ethics Committee (ethics number 17-014 UM). At UCLA, all procedures were approved by the University of California Los Angeles Institutional Animal Care and Use Committee (protocol 2000-153-61 A) (for more details see Ndode-Ekane et al., 2019; this supplement).

2.2. Induction of lateral fluid percussion injury (FPI) and electrode implantation

TBI was induced by lateral FPI, as described by Ndode-Ekane et al. (2019). Briefly, rats were anesthetized using 5% isoflurane. A craniectomy (Ø 5 mm) was performed with a trephine (UEF, UCLA) or hand-held drill (Melbourne) centered from bregma: AP -4.5 mm and 2.5 in the ML axis over the left cortex. After the bone was removed the dura was inspected to ensure it was intact. Next, a modified Luer-Lock syringe cap was anchored over the craniectomy and set with dental acrylate. An anterior dental screw was placed and set as well. Then, TBI was induced with a fluid-percussion device equipped with a straight-tip attachment (AmScien Instruments, Model FP 302, Richmond, VA, USA,). The pressure level was adjusted to produce a severe TBI with a target mortality between 20 and 30% within the first 48 h (Pitkanen and McIntosh, 2006). Sham-operated experimental controls underwent the same surgical procedures as the TBI rats including placement of the luer-lock and anchor screw, but TBI was not induced. The rat was removed from the device and placed on a heating pad immediately after the impact. In Melbourne, all of the rats received medical oxygen (Mediquip Pvt Ltd. Australia) at 0.5 l/min to aid oxygenation until the rat regained a regular breathing pattern (for more details see Ndode-Ekane et al., 2019).

At UEF and UCLA bipolar depth electrodes and extradural cortical electrodes were implanted during the same surgery as the injury. Electrode locations are summarized in Fig. 1. Bipolar electrodes with tip separation of 1 mm were implanted in the perilesional cortex fronto-parietal ($Y_{1,2}$: AP = -1.7, ML = 4.0 and D = -1.8) and posterior to the craniotomy ($X_{1,2}$: AP = -7.6, ML = 4.0 and D = -1.8). An additional bipolar electrode was implanted in the anterior ipsilateral hippocampus, aiming at the distal CA1 ($H_{1,2}$: AP = -3.0, ML = 1.4 and D = -3.6). Four epidural screw electrodes were implanted into ipsilateral fronto-parietal (C3: AP: -1.7; ML: 2.5), contralateral fronto-parietal (C4: AP: 1.7; ML: 2.5), ipsilateral occipital (O1: AP: -7. 6; ML: 2.5) and contralateral occipital (O2: AP: -7.6; ML: 2.5) area (Paxinos and Watson, 2007). Ground and reference electrodes (stainless steel screws) were inserted in the skull bone overlying the cerebellum (Figs. 1 and 2). In Melbourne, the electrode implantation was performed 24 h after the TBI induction. The electrodes were mounted in a 12-channel Plastics One pedestal (Roanoke, VA) and connected to the inputs. Details of cables and connectors are summarized in Tables 1 and 2.

For the purpose of this paper, only data from the 28-day EEG were included in the analysis. It is important to mention that a separate cohort of rats received a series of Magnetic Resonance Imaging (MRI) after TBI. The same electrodes and placements were used, but surgical implantation was performed 6 months after TBI at all three sites (Fig. 2; for more details see Ndode-Ekane et al., 2019).

2.3. Data acquisition

Immediately following surgery, rats were placed in a cage with temperature-regulated mat and monitored during recovery before being returned to the home cage (around 30 min). Then, EEG recording began within an hour after completion of the surgery (about 2 h after the impact in UEF and UCLA, 24 h in Melbourne) and was performed continuously 24 h/day for the first week after TBI. Thereafter, EEG recordings were performed for the first two days of every month for the first 5 months. On the 6^{th} month, EEG monitoring was continuous (24/7) for the entire month. EEG was sampled at a minimum of 2 kHz per channel and minimum passband between 0.1 Hz and 1 kHz. EEG was recorded referentially to a screw electrode positioned in the skull overlying the right cerebellar cortex. The components of the EEG systems and recording settings for each of the sites are listed in Tables 1 and 2.

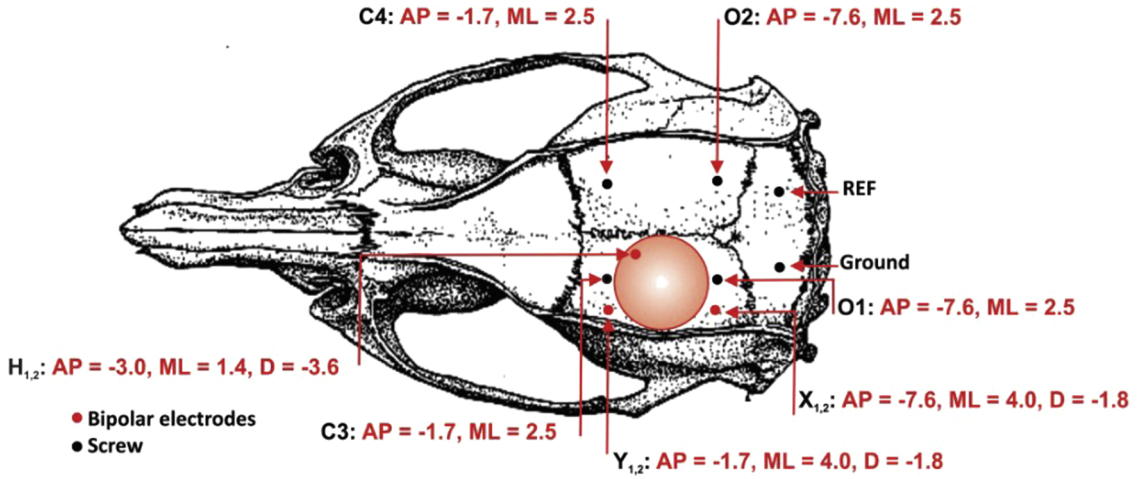

Fig. 1. Electrode placements for EEG recording (adapted from Paxinos and Watson, 2007). All the sites used the same coordinates and similar electrodes types for the recording. Note that electrodes were positioned anterior, medial, and posterior to the craniotomy (orange circle) which is dorsal to actiual lesion core that is typically in the auditory cortex (see Fig. 2). Abbreviations: O1, ipsilateral occipital; O2, contralateral occipital; C3, ipsilateral fronto-parietal; C4, contralateral fronto-parietal; $Y_{1,2}$, bipolar fronto-parietal; $X_{1,2}$, bipolar ipsilateral occipital; $H_{1,2}$, bipolar hippocampus and REF; reference.

2.4. Data selection

For assessing HFO detection algorithms, four 10-minute EEG files (UEF and UCLA each had one TBI and on sham-injured control rat) recorded 28 days post-impact were selected. EEG contained predominately high-amplitude slow wave activity typical of the N2/N3 sleep state. The files were visually inspected to exclude periods that were contaminated with movement and muscle-related artifacts. Additionally, power spectral analysis (Fast Fourier Transform) was used to identify channels with power line noise (50 or 60 Hz and harmonics). Channels containing appreciable levels of power line noise were excluded from all subsequent analysis. Data processing details are presented in Table 3.

2.5. Approach for automated HFOs detection

After the data selection, each center carried out a computer-automated analysis of HFOs for each channel in the selected files. At UEF, HFOs detection was performed using an in-house Matlab script. Briefly the algorithm consisted of the following steps:

1 Bandpass filtering (ideal digital filter) of raw signal between 80 and 500 Hz. To filter the signal, we take the Fourier transformation from the real time signal and remove the frequency band that we want get rid off. Then, we take the inverse Fourier transform back to the real time (without the unwanted band or bands).
2 Calculation of the mean spectral power of the filtered signal using overlapped windows, in which we calculate the mean power of this window, furthermore we calculate mean of these mean power and the standard deviation.
3 Analysis of channels using the Hilbert transforms.
4 Expansion of window t1 (one second) which center is t0 (start time high power window in step 2).
5 Take a window tw2 = [t0-0.5 s, t0]; calculate the average value of analytical signal, and the absolute value of the filtered signal.
6 On time window t1 we look where the analytical signal rises over the threshold value (twice as the average value calculated on window tw2) this indicates the starting time of the HFO candidate, then time point when the analytical signal drops below the threshold is calculated indicating the end of the HFO candidate. This leads to the duration (tw3) of the HFO candidate.
7 Using a derivative, find the number of the peaks on time window tw3 calculated in step 6 of the filtered signal on those events found in step 6 "Choose the events" which have more than 8 peaks (4 cycles) higher than 2 times the mean peak value (calculated in step 5).

For Melbourne and UCLA, the HFOs detection was performed using

Table 2
EEG Amplifiers and Settings.

	UEF	Melbourne	UCLA
Amplifier Model	Digital Lynx 16SX (Neuralynx, USA)	Neuvo	Intan RHD2000
Acquisition software	Cheetah ver. 6.3.2	Profusion EEG 5	RHD2000
Sampling rate	10kHz	2KHz/channel	2KHz/channel
Filter settings	FIR high-pass 0.1Hz	0.01-2030 Hz	0.1-1000 Hz
EEG file format	.NCS converted to EDF +	.rda2 converted to EDF +	.RHD converted to EDF +
EEG file duration	24h	24 h	2 h
EEG file size	~18 GB	~3.8 GB	~1.2 GB

Table 1
Components of the Tethered EEG System.

	UEF	Melbourne	UCLA
Head Cap	Pedestal 12Ch – (MS12P EM12/20/2.4/SP)	12-channel pedestal (MS12 P EM12/20/2.4/SP	12-channel pedestal (MS12 P EM12/20/2.4/SP)
Cable	Flexible shielded cable (M12C-363/2, PlasticsOne Inc.)	Flexible shielded cable (M12C-363/2, PlasticsOne Inc.)	Flexible shielded cable (M12C-363/2, PlasticsOne Inc.)
Commutator	12-pin swivel (SL12C, 12-pin swivel (SL12C, PlasticsOne Inc.)	12-channel double-brush (SL-12C, 12-pin swivel (SL12C, PlasticsOne Inc.)	12-channel double-brush (SL-12C, 12-pin swivel (SL12C, PlasticsOne Inc.)
Electrode material and impedance	Initially below 5KΩ Maintained below 10KΩ	Below 10KΩ (measured at 1000 Hz)	Pogo-contact Below 5KΩ

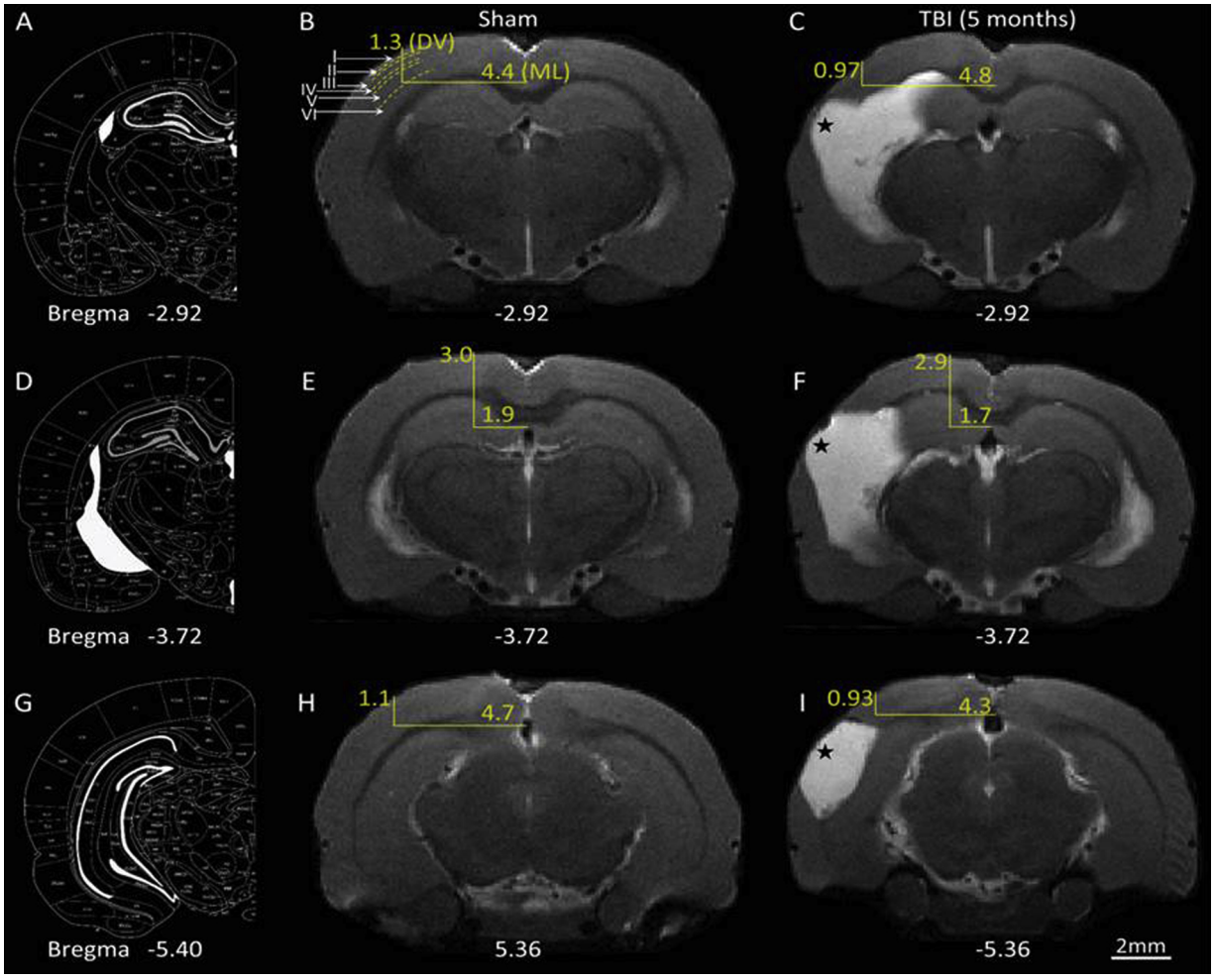

Fig. 2. Adjustment of coordinates for chronic electrode implantation due to post-injury brain atrophy and deformation. Atlas plates and T2 weighted magnetic resonance images (MRI) slices demonstrating the anteroposterior (AP), medialateral (ML) and dorsoventral (DV) coordinates of the anterior cortical (Panel A–C), hippocampal (Panel D–F) and posterior cortical (panel G–I) intracranial bipolar electrode in a rat with sham-operation and lateral fluidpercussion-induced traumatic brain injurury (TBI) 5 months earlier (MRI cohort). (A) Atlas plate depicting the approximate AP coordinate (bregma as reference) of the anterior cortical electrode (rat brain atlas of Paxinos and Watson, 2007). (B) The ML and DV coordinate of the anterior cortical electrode in a sham rat. Note the tip of the electrode in layer V. (C) The ML and DV coordinate of anterior cortical electrode in a TBI rat. Note the reduced length of the DV coordinate due to post-injury cortical atrophy. The star represents the approximate location of the core of the cortical lesion. In this TBI case, the lesion cavity is filled with cerebrospinal fluid that appears bright in MRI. (D) The AP coordinate of the hippocampal electrode as estimated from the atlas. (E) The ML and DV coordinate of the hippocampal electrode in the sham rat. (F) The ML and DV coordinate of the hippocampal electrode in the TBI rat. Note the hippocampal deformation and expanding ventricle. (G) The AP coordinate of the posterior cortical electrode. (H) The ML and DV coordinate of the posterior cortical electrode in the sham rat. Note that the cortical thickness is still more than 1 mm. (I) ML and DV coordinate of the posterior cortical electrode in the TBI rat. The ML coordinate is less than in the sham rat. All the AP, ML and DV values are shown in millimeters (mm). Scale bare equals 2 mm.

Table 3
EEG files details.

	UEF	Melbourne	UCLA
Data acquisition and analysis of signal quality	Visual review, impedance check, automated detection signals with 50 Hz and harmonics	Manual review with FFT analysis using custom-written MATLAB scripts for 50 Hz and harmonics	Manual review with FFT analysis for 60 Hz and harmonics
File review and select artifact-free episodes	Visual inspection with spike2 and automatic ID of epochs with amplifier saturation	Manual review/selection using custom-written MATLAB scripts	Manual review and select with EDF Browser
HFO detection and verification	Semi-automated with Matlab algorithm; visual review with rules-based approach	Semi-automated with RippleLab; Short-term energy algorithm and review with rules-based approach	Semi-automated with RippleLab; Short-term energy algorithm and review with rules-based approach
Output file format	Text (*.txt;*.cvs) and/or Matlab, Excel files	Matlab (*.mat) and Excel files	Matlab (*.mat) and Excel files
Raw data file storage	Group NAS, LONI IDA	Melbourne shared Drive and LONI IDA	Upload UCLA Box and LONI IDA

RippleLab software (Matlab-based) (Navarrete et al., 2016). HFOs were detected using the Short Time Energy (STE) algorithm proposed by Staba et al. (2002), using the following parameters: band pass filter 80–500 Hz, successive root mean square (RMS) values greater than 5 standard deviations (SD) above the overall RMS mean within 3 ms window. Putative HFOs events were then selected if they lasted more than 6 ms and contained more than 8 peaks (4 oscillations) greater than 3 SD (Melbourne; 2 SD was used at UCLA) above the mean value of the rectified band-pass signal. In addition, events separated by 10 ms or less were marked as a single oscillation.

2.6. Post-processing criteria for review

After the automated detection process, all putative HFO events were reviewed manually using the following criteria agreed upon by all 3 sites. EEG was displayed in a 500 msec window with the raw or unfiltered EEG signal above the bandpass filter signal (80–500 Hz). The gain of the bandpass filtered signal was set to a minimum of 2 times the unfiltered EEG signal. The frequency displayed in spectrogram was between 80 and 500 Hz.

Criteria:

- Sinusoid-like waveform between 80–500 Hz in the unfiltered signal that is distinct from surrounding background activity.
- Minimum of four recurrent waves or cycles in unfiltered data.
- Amplitude greater than 2 times surrounding average baseline (minimum of 0.2 s before and after putative HFO) in the filtered signal.
- Alignment of peaks with peaks and troughs with trough between the unfiltered EEG signal and bandpass filter signal (80–500 Hz).
- Dominant peak (or local maximum) in power of the spectrogram limited between 80–200 and / or 200–500 Hz.

Events that met at least one of the following exclusion criteria were considered as false positives:

- Association with sharp voltage transients in EEG due to movement or muscle artifact (e.g. chewing).
- Event present simultaneously on three or more electrodes.
- Event due to filtered neuronal spikes.

3. Results

3.1. Surgery for impact and electrode implantation

Review of the surgical reports showed that at UEF 45 rats were randomized to TBI or sham-injury (37 TBI and 8 shams) with a 16% (6/37) post-impact mortality rate. The mean impact pressure was (2.79 ± 0.14 atm). At Melbourne randomization produced 32 TBI and 7 shams rats with a post-impact mortality rate of 59% (19/32). The mean impact pressure at Melbourne was 2.41 ± 0.21 atm. At UCLA randomization produced 32 TBI and 7 shams rats with a post-impact mortality of 59% (19/32). The mean impact pressure at UCLA was 2.37 ± 0.18 atm. All sites rats had an intact dura in both TBI and sham-injured groups, and electrodes were implanted in the same position according to the coordinates illustrated in Fig. 1. Details of the FPI and post-injury monitoring are described by Ndode-Ekane et al. 2019 (in this issue).

3.2. Criteria for inclusion and exclusion of data quality

Each study site analyzed four 10-minute EEG files that were recorded from four separate rats (2 TBI, 2 sham-injured) located at UEF and UCLA. At the time of this report recordings from Melbourne were not available due to technical issues with the EEG files. Visual inspection of the unprocessed EEG found evidence of putative HFOs in both epidural screw electrodes and in paired, microwire electrodes positioned in the perilesional cortex and ipsilateral hippocampus.

Some electrodes had a poor signal quality due to technical issues and were removed from analysis (Fig. 3, see channel H2). All remaining channels from each of the four EEG files were analyzed for putative HFOs using two semi-automated computer algorithms; one an in-house Matlab-based script designed at UEF and the other RippleLab used at UCLA and Melbourne (Navarrete et al., 2016)(see Section 2.5). Detected events were then visually validated.

3.3. Total HFOs detections

3.3.1. Algorithm

Altogether, the unsupervised computer algorithms detected 266 events in UEF, 782 events Melbourne, and 771 events at UCLA (Fig. 4). Of the total number of detections, 40 events were detected by algorithms at all three sites. There were 26.0% (360 events) detected events in common between UCLA and Melbourne, 4.3% (60 events) in common between UCLA and UEF, and 4.1% (57 events) in common between Melbourne and UEF (Fig. 4A).

Further inspection of the events showed that 56.4% (780) were recorded in one sham-injured rat from UEF. Most of these events were detected on electrodes positioned in the ipsilateral hippocampus (e.g. $H_{1,2}$ in Figs. 1 and 2) and in the deeper of the paired electrodes positioned in the perilesional cortex ($Y_{1,2}$).

3.3.2. Manual post-processing validation

Each center manually reviewed all of their detected events to determine whether or not each event was an HFO (i.e., true positive) according to the criteria listed in the Methods (see Section 2.6). Of the total events detected the three sites classified 130 events as HFOs and the remaining 1,252 events as false positives (Fig. 4B-C). Of the 40 events detected by all three sites, sites all agreed 10 were HFOs and 25 were false positives and disagreed on the remaining 5 events (Figs. 4 and 5). This represents 87.5% agreement between all three sites. Comparison of the detected events in common between two sites found the highest level of agreement between UEF and Melbourne (55 events or 96.5%), intermediate agreement between UCLA and Melbourne (311 events or 86.3%), and the lowest agreement between UEF and UCLA (35 events or 58.3%; Fig. 4). The mean (+/- SD) rate of HFO occurrence per rat at each center was 0.27 ± 0.55 events/min at UEF, 0.08 ± 0.17 events/min at Melbourne and 0.05 ± 0.13 events/min at UCLA. Representative examples of the detected events and events classified as HFOs are illustrated in Figs. 5 and 6 respectively.

4. Discussion

This first report from the EpiBioS4Rx Consortium demonstrates the standardized placements of epidural and intracerebral electrodes used to record EEG in TBI and sham-injured rats. Twenty-eight days after electrode implantation, EEG files from 2 of the 3 centers contained bursts of HFOs similar to those found in status-epilepticus models of chronic epilepsy. Different computer-automated detection algorithms and small changes in detection parameters produced different results, and common review criteria can help eliminate spurious EEG events and verify HFOs. These data indicate progress and identified areas for improvement in the evaluation of HFOs as an electrophysiological biomarker of PTE in a multi-center design.

Our first objective was to establish consistent placement of electrodes above and within peri-lesional tissue, which is critical for combining data across sites. Consistent placements will also help to record comparable EEG signals since differences in distances between recording electrode and cellular sources generating HFO, presumably within and around the lesion, can greatly affect the amplitude and morphology of the HFO waveform (Bragin et al., 2007). We also used a common reference site for referential recording and a referential

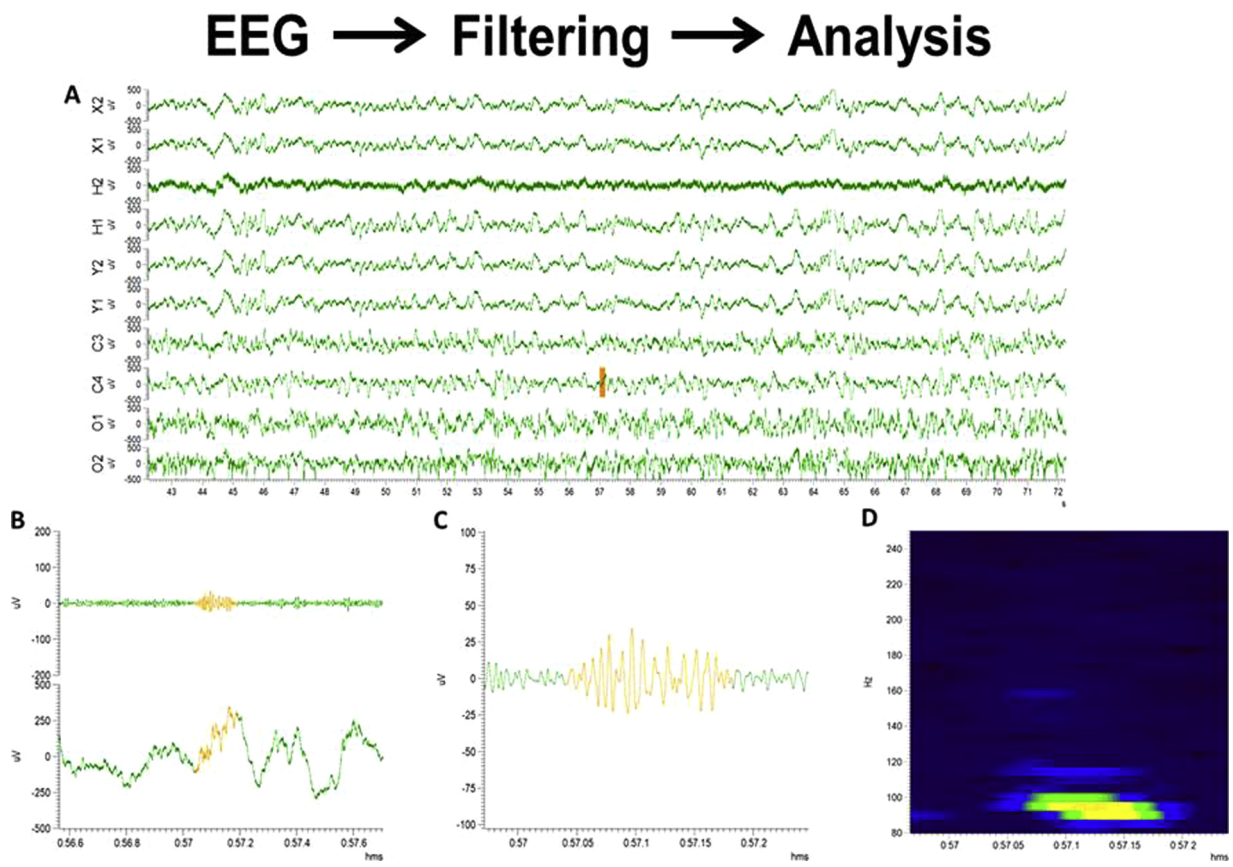

Fig. 3. An example of a true positive high-frequency oscillation (HFO) in a rat with lateral fluid-percussion induced TBI 5 weeks earlier in UEF. See the methods section for electrode placements. Notice that electrode at the position H2 does not present any valid signal due to a bad connection between the pogo-pin at the pedestal and the connector in the cable. (A) A 30-seconds epoch showing in orange the localization of the identified HFO in C4 during sleep stage N3. (B) Upper tracing: unfiltered signal. Lower tracing: filtered signal in the same time scale (marked in orange in panel A). (C) Magnification of the filtered signal fulfilling the criteria set for a HFO. (D) A heat map of the identified HFO showing maximum power between 85 and 100 Hz.

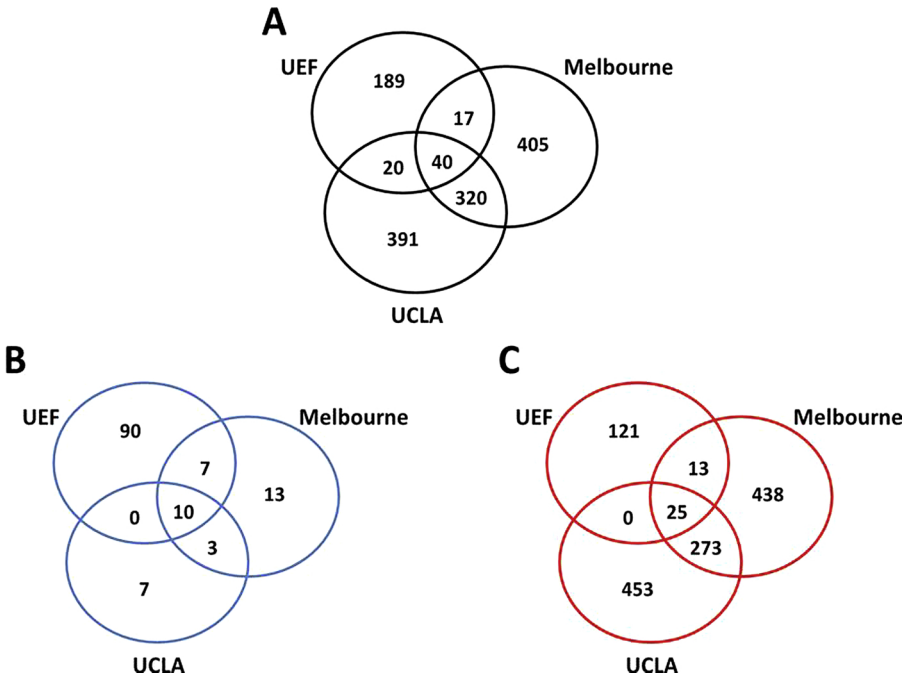

Fig. 4. Venn diagrams illustrating the total number of putative high-frequency oscillations (HFOs), true positives, and false positives. (A) All events detected by computer algorithms: UEF and Melbourne/UCLA computer based unsupervised algorithms detected a total of 1,819 putative HFOs in two sham-operated experimental controls and in two rats with lateral fluid-percussion induced traumatic brain injury (TBI). From these, 266 were found in UEF, 782 in Melbourne and 771 in UCLA. Numbers in overlapping areas represent the number of events that were in common between two or all three sites. The numbers in non-overlapping areas show the number of events detected by that site only. (B) True positives after visual analysis: All detected events were manually reviewed and classified as true positives (i.e. HFOs) or false positives. Thus, 40% (107 of 266) of HFOs detected by UEF algorithm and visually verified in UEF, 4% (33 of 782) of HFOs detected by UCLA/Melbourne algorithm and visually verified by Melbourne, and 3% (20 of 771) of HFOs detected by UCLA/Melbourne algorithm and visually verified by UCLA were considered true positives. From the total of 130 visually verified true positive HFOs, 10 (8%) were common for all three study sites. (C) False positives after visual analysis: Visual analysis indicated that 60% of the algorithm-detected putative HFOs were false positives in UEF, 96% in Melbourne, and 97% in UCLA. From the total of 1323 false positives events, 25 (2%) were common to all sites.

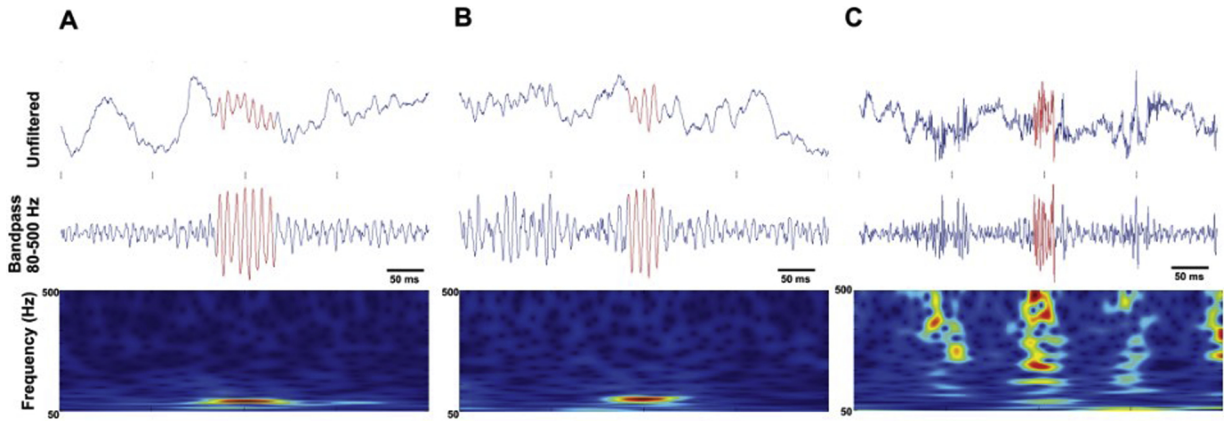

Fig. 5. Representative EEG examples of the events detected from the three sites. (A) An event that all three sites classified as an HFO (true positive). (B) EEG event that the sites disagreed. (C) An event detected by both the UEF and Melbourne/UCLA algorithms that in consequent visual analysis was classified as a false positive by all three sites. Upper panels: unfiltered signal. Middle panels: bandpass 80–500 Hz tracing. Lower panels: power spectrum corresponding to the filtered signal. Notice that difference between true positives (A) and events of disagreements (B) often were associated with an ambiguous number of cycles and/or the amplitude of the event was not two time greater than the surrounding EEG background.

montage for data analysis to reduce issues that could combine or cancel HFO signals recorded on two different electrodes (Menendez de la Prida et al., 2015).

Our results demonstrate our electrodes and EEG systems designed for long-term monitoring are capable of recording bursts of HFOs generated in the perilesional cortex and ipsilateral hippocampus at least

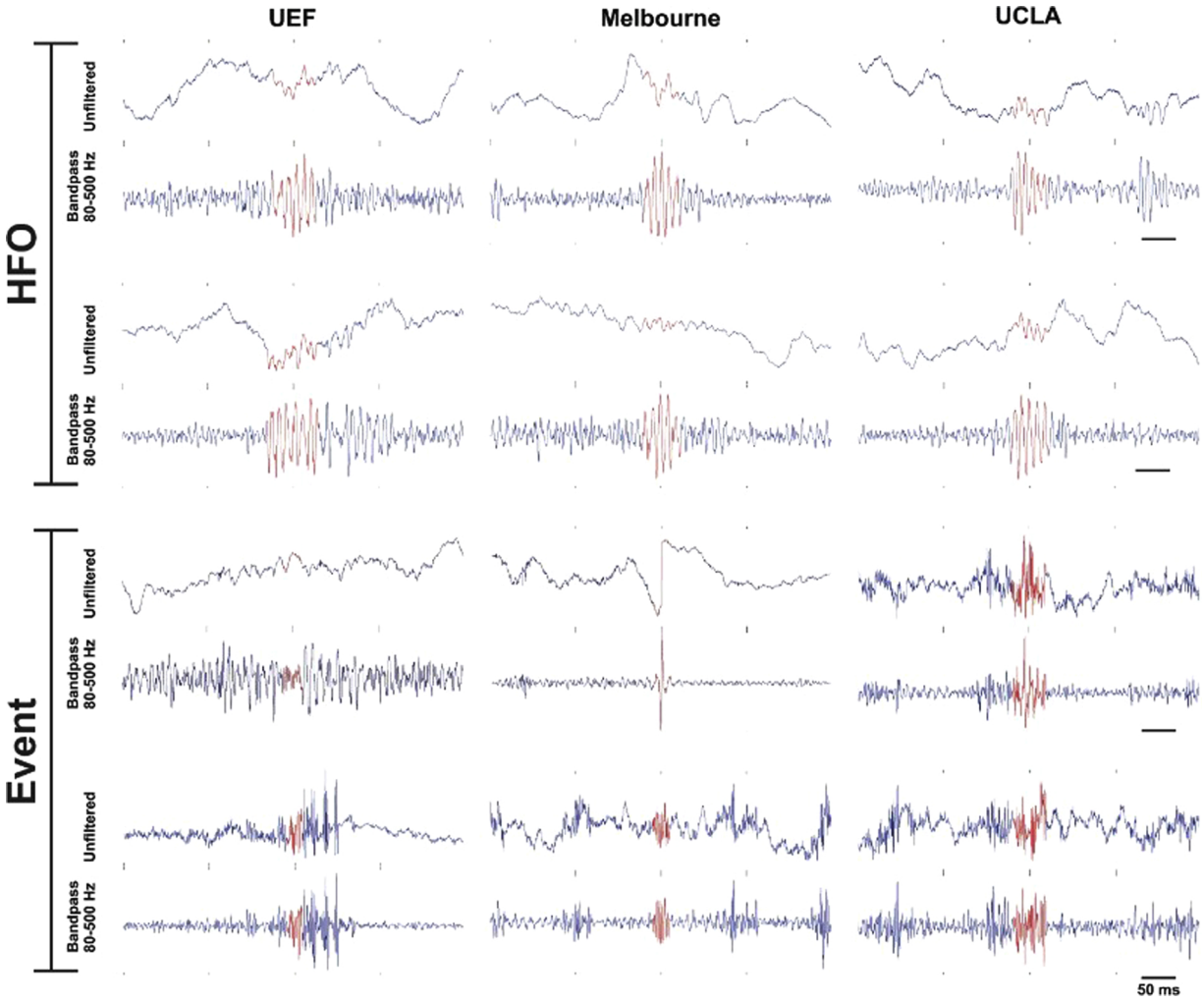

Fig. 6. Representative EEG examples of algorithm-detected HFOs (top half) and events classified as false positives (bottom half) at one site that were not detected by the other sites. Note that all HFOs contain at least four recurrent waves or cycles in unfiltered data with amplitude greater than 2 times surrounding baseline in accordance with the inclusion criteria previously described in the methodology section. Regarding the false positives detected, notice the association with sharp voltage transients in EEG due to movement or muscle artifact, (e.g. chewing) in accordance with the exclusion criteria previously described (see the methods section).

28 days post-injury. We were able to record EEGs with HFOs that are similar in waveform morphology and amplitude between 2 of the 3 sites. One of the sites had technical issues converting the native file format to the common EDF + format needed for the detection software, illustrating how a minor practical problem can introduce delays in the research. All of the sites, however, had similar recording issues (e.g. power line noise, high impedance electrode or reference) that affected signal quality on some electrodes and recordings contained movement and muscle-related artifacts. As part of our protocol channels contaminated with power line noise and EEG episodes containing substantial artifacts were identified and removed from the analysis. Transient artifacts did occur and were detected by our algorithms, but each of the sites could consistently identify these artifacts by using the manual review criteria.

The majority of events were detected by one of the two algorithms used in this preliminary. Most of events were classified as false positives, which is common in HFO studies (Amiri et al., 2016; Weiss et al., 2018). Differences in the number of false positives is less of an issue aside from the time required to remove these events from further analysis. As this report showed, the selection of different algorithms to detect HFOs can produce very different results in the number of HFOs. Our next steps forward will be to establish a “ground truth” dataset containing labeled events all sites agree are HFOs and each site can use this dataset to assess and improve the performance of their detection algorithm. Alternatively, we could consider using one common algorithm, selecting on set of detection parameters, and validating its performance against a ground truth dataset. Even in our sample we observed that despite two sites using the same algorithm, seemingly minor changes in the parameter values (2 vs 3 SD threshold setting) can produce differences in the detections. Thus, one set of parameters and strict adherence to these values could reduce variability.

There were 40 events in the EEG recordings that were detected by both the UEF and Melbourne/UCLA algorithms. Ten of these events were verified as HFO and 25 as false positives by all three sites. This level of agreement between sites is acceptable for this stage and is expected to improve with additional practice, considering that the investigators performing this analysis had very little or no prior experience with studies of HFOs. There are different types of HFOs (e.g. burst and sustained oscillations, hippocampal and neocortical; see Jefferys et al., 2012) and no universal definition or criteria to verify their occurrence in the EEG. We are also aware that properties of HFOs (e.g. duration, spectral energy) could evolve during the development of epilepsy (Jones et al., 2015). We have selected computational approaches commonly used to detect HFOs and developed a manual review strategy that would be practical, account for the evolution of HFOs (if any), and could be reliably implemented (Navarrete et al., 2016). Our results suggest we need to revisit and possibly revise some of the criteria, especially the minimum amplitude criterion of 2 times the mean baseline activity 200 msec before and after the event. In some cases, the baseline contained increased neuronal activity or other bursts of HFOs, and thus, it was unclear whether or not the amplitude of each complete cycle of the putative HFO was 2 times greater. We will collect a dataset of HFOs and spurious events and collectively review the examples to help investigators understand and implement the review criteria. An alternative strategy might be to maintain the exclusion criteria, but remove the minimum number of cycles, amplitude, and power requirements from the inclusion criteria. In this approach, all obvious artifacts would be removed and HFO and its variants retained. The retained events could then be labeled with respect to the confidence of HFO (e.g. definite and possible or high, moderate, and low) (Spring et al., 2017).

5. Conclusions

Harmonizing the recording and detection of HFOs is crucial in the EpiBioS4Rx multi-center studies in order to establish robust, clinically translatable electrophysiological biomarkers of PTE. Our interim analysis found variability in the detection and review of HFOs that can be attributed to (1) the EEG signal quality, (2) the choice of algorithm and parameters used to detect HFOs, and (3) the manual review criteria for verifying HFOs. Reducing the variability between sites will involve additional investigator training, consideration of single or multiple detection algorithms, test datasets to improve performance of detection algorithms, and unequivocal review criteria to validate HFOs and exclude artifacts.

Acknowledgement

This research was supported by the National Institute of Neurological Disorders and Stroke (NINDS) Center without Walls of the National Institutes of Health (NIH) under Award Number U54NS100064 (EpiBioS4Rx).

References

Amiri, M., Lina, J.M., Pizzo, F., Gotman, J., 2016. High Frequency Oscillations and spikes: separating real HFOs from false oscillations. Clin. Neurophysiol. 127, 187–196. https://doi.org/10.1016/j.clinph.2015.04.290.

Annegers, J.F., Hauser, W.A., Coan, S.P., Rocca, W.A., 1998. A population-based study of seizures after traumatic brain injuries. N. Engl. J. Med. 338, 20–24. https://doi.org/10.1056/NEJM199801013380104.

Bragin, A., Wilson, C.L., Engel, J., 2000. Chronic Epileptogenesis Requires Development of a Network of Pathologically Interconnected Neuron Clusters: A Hypothesis. Epilepsia 41, S144–S152. https://doi.org/10.1111/j.1528-1157.2000.tb01573.x.

Bragin, A., Wilson, C.L., Almajano, J., Mody, I., Engel, J., 2004. High-frequency oscillations after status epilepticus: epileptogenesis and seizure genesis. Epilepsia 45, 1017–1023. https://doi.org/10.1111/j.0013-9580.2004.17004.x.

Bragin, A., Wilson, C.L., Engel, J., 2007. Voltage depth profiles of high-frequency oscillations after kainic acid-induced status epilepticus. Epilepsia 48, 35–40. https://doi.org/10.1111/j.1528-1167.2007.01287.x.

Jacobs, J., Staba, R., Asano, E., Otsubo, H., Wu, J.Y., Zijlmans, M., Mohamed, I., Kahane, P., Dubeau, F., Navarro, V., Gotman, J., 2012. High-frequency oscillations (HFOs) in clinical epilepsy. Prog. Neurobiol. 98, 302–315. https://doi.org/10.1016/j.pneurobio.2012.03.001.

Jefferys, J.G.R., Menendez de la Prida, L., Wendling, F., Bragin, A., Avoli, M., Timofeev, I., Lopes da Silva, F.H., 2012. Mechanisms of physiological and epileptic HFO generation. Prog. Neurobiol. 98, 250–264. https://doi.org/10.1016/j.pneurobio.2012.02.005.

Jiruska, P., Alvarado-Rojas, C., Schevon, C.A., Staba, R., Stacey, W., Wendling, F., Avoli, M., 2017. Update on the mechanisms and roles of high-frequency oscillations in seizures and epileptic disorders. Epilepsia 58, 1330–1339. https://doi.org/10.1111/epi.13830.

Jones, R.T., Barth, A.M., Ormiston, L.D., Mody, I., 2015. Evolution of temporal and spectral dynamics of pathologic high-frequency oscillations (pHFOs) during epileptogenesis. Epilepsia 56, 1879–1889. https://doi.org/10.1111/epi.13218.

Lévesque, M., Bortel, A., Gotman, J., Avoli, M., 2011. High-frequency (80-500 Hz) oscillations and epileptogenesis in temporal lobe epilepsy. Neurobiol. Dis. 42, 231–241. https://doi.org/10.1016/j.nbd.2011.01.007.

Menendez de la Prida, L., Staba, R., Dian, J.A., 2015. Conundrums of high-frequency oscillations (80-800 Hz) in the epileptic brain. J. Clin. Neurophysiol. 32, 207–219. https://doi.org/10.1097/WNP.0000000000000150.

Navarrete, M., Alvarado-Rojas, C., Le Van Quyen, M., Valderrama, M., 2016. RIPPLELAB: a comprehensive application for the detection, analysis and classification of high frequency oscillations in electroencephalographic signals. PLoS One 11. https://doi.org/10.1371/journal.pone.0158276.

Paxinos, G., Watson, C., 2007. The Rat Brain in Stereotaxic Coordinates, 6th edn. ed. Academic Press/Elsevier, Amsterdam ; Boston.

Pitkanen, A., McIntosh, T., 2006. Animal models of post-traumatic epilepsy. J. Neurot 23, 241–261.

Spring, A.M., Pittman, D.J., Aghakhani, Y., Jirsch, J., Pillay, N., Bello-Espinosa, L.E., Josephson, C., Federico, P., 2017. Interrater reliability of visually evaluated high frequency oscillations. Clin. Neurophysiol. 128, 433–441. https://doi.org/10.1016/j.clinph.2016.12.017.

Weiss, S.A., Berry, B., Chervoneva, I., Waldman, Z., Guba, J., Bower, M., Kucewicz, M., Brinkmann, B., Kremen, V., Khadjevand, F., Varatharajah, Y., Guragain, H., Sharan, A., Wu, C., Staba, R., Engel, J., Sperling, M., Worrell, G., 2018. Visually validated semi-automatic high-frequency oscillation detection aides the delineation of epileptogenic regions during intra-operative electrocorticography. Clin. Neurophysiol. 129, 2089–2098. https://doi.org/10.1016/j.clinph.2018.06.030.